Role of the Chain Termini for the Folding Transition State of the Cold Shock Protein[†]

Dieter Perl,[‡] Georg Holtermann,[§] and Franz X. Schmid*[,‡]

Laboratorium für Biochemie und Bayreuther Zentrum für Molekulare Biowissenschaften, Universität Bayreuth, D-95440 Bayreuth, Germany, and Abteilung Physikalische Biochemie, Max-Planck-Institut für molekulare Physiologie, D-44202 Dortmund, Germany

Received July 2, 2001; Revised Manuscript Received October 2, 2001

ABSTRACT: Residues Arg3 and Leu66 are crucially important for the enhanced stability of the cold shock protein *Bc*-Csp from the thermophile *Bacillus caldolyticus* relative to its homologue *Bs*-CspB from the mesophile *Bacillus subtilis*. Arg3, which replaces Glu3 of *Bs*-CspB, accounts for two-thirds of the stability difference and for the entire difference in Coulombic interactions between the two proteins. Leu66, which replaces Glu66 of *Bs*-CspB, contributes additional hydrophobic interactions. To elucidate the role of these two residues near the chain termini for the rapid folding of the cold shock proteins, we performed an extensive mutational analysis of the folding kinetics to characterize interactions between residues 3, 46, and 66 in the transition state of folding. We employed a pressure-jump apparatus which allows folding to be followed over a broad range of temperatures and urea concentrations in the time range of microseconds to minutes. The N-terminal region folds early, and the interactions that originate from residue 3 are present to a large extent in the transition state already. They include a hydrophobic contribution, a general electrostatic stabilization by the positive charge of Arg3 in *Bc*-Csp, and a pairwise Coulombic repulsion with Glu46 in the Arg3Glu variant. The C-terminus appears to be largely unfolded in the transition state. The interactions of Leu66, including those with the already structured N-terminal region, are established only after passage through the transition state. The N- and C-termini of the cold shock proteins thus contribute differently to the folding kinetics, although they are very close in space in the folded protein.

To understand the mechanism of protein folding, it is necessary to elucidate the energetic and structural properties of partially folded intermediates and of the activated or transition states, which control the rate of folding. Folding transition states are most easily investigated for proteins that fold in U ⇌ N two-state reactions, because the analysis is not complicated by the population of folding intermediates (*1*−*6*). The thermodynamic properties of folding transition states and their location along the reaction coordinate usually vary between proteins, but mutational analyses of the folding of proteins, such as chymotrypsin inhibitor 2 (CI2) (*7*) or several SH3 domains (*8*, *9*), indicated that transition states represent small ensembles of well-defined structures in which some chain regions are folded already, whereas others are still unfolded (for a recent review, see ref *6*). These findings agree better with the traditional view of protein folding proceeding along defined pathways (*10*−*12*) than with funnel-type folding where many different routes are available for a protein molecule to reach its native state (*13*−*15*).

The contributions of individual residues to the energy of the transition state can be elucidated by mutational studies of the unfolding and refolding kinetics as a function of the temperature and the solvent composition. A residue is assumed to be in a nativelike region of the transition state when mutations of this residue change the equilibrium Gibbs free energy ΔG_D[1] and the Gibbs free energy of activation for refolding $\Delta G^{\ddagger}_{UN}$ to the same extent. Conversely, when the changes in ΔG_D and in the activation energy for unfolding $\Delta G^{\ddagger}_{NU}$ are equal, the mutated residue is assumed to reside in an unfolded region of the activated state. This analysis was pioneered by the Matthews group (*16*) and cast into the popular Φ value analysis by Fersht (*17*, *18*). In these treatments, it is assumed that the mutations do not affect the unfolded state. Interactions between specific sites and their importance for the transition state can be elucidated by double-mutant analyses (*19*, *20*). Studies of homologous proteins with different conformational stabilities are useful for examining the evolutionary conservation of folding pathways and for elucidating the relationship between an equilibrium stability and folding mechanism (*21*).

The cold shock proteins from the mesophiles *Escherichia coli* (*22*) and *Bacillus subtilis* (*Bs*-CspB), the thermophile *Bacillus caldolyticus* (*Bc*-Csp), and the hyperthermophile

[†] This work was supported by grants from the Deutsche Forschungsgemeinschaft and the Fonds der Chemischen Industrie.

* To whom correspondence should be addressed: Universität Bayreuth, D-95440 Bayreuth, Germany. Telephone: ++49 921 553660. Fax: ++49 921 553661. E-mail: fx.schmid@uni-bayreuth.de.

[‡] Universität Bayreuth.

[§] Max-Planck-Institut für molekulare Physiologie.

[1] Abbreviations: *Bs*-CspB and *Bc*-Csp, cold shock proteins from *B. subtilis* and *B. caldolyticus*, respectively; GdmCl, guanidinium chloride; N and U, folded and unfolded forms of the protein, respectively. Proteins from mesophilic and thermophilic organisms are denoted as mesophilic and thermophilic proteins, respectively. The equilibrium thermodynamic parameters for denaturation are denoted with the subscript D. The activation parameters for refolding and unfolding are denoted with the subscripts UN and NU, respectively.

10.1021/bi011378s CCC: $20.00
Published on Web 12/01/2001

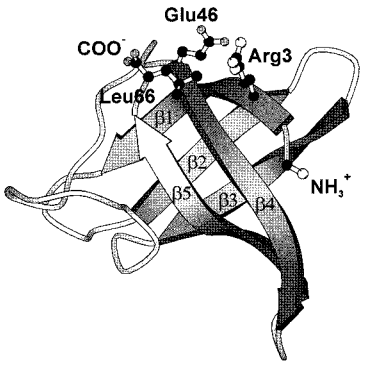

FIGURE 1: Ribbon drawing of the tertiary structure of *Bc*-Csp. Five antiparallel β-strands (numbered) form a β-barrel structure. This Molscript figure (*41*) is based on the coordinates of ref *25*. The side chains of residues Arg3, Glu46, and Leu66, as well as the N- and C-termini, are shown in ball-and-stick representation.

Thermotoga maritima (*Tm*-Csp) (*23*) share a very rapid N $\rightleftharpoons$ U two-state folding reaction with a nativelike folding transition state, although these proteins differ significantly in stability. The differences in stability between *Bs*-CspB and *Bc*-Csp ($\Delta\Delta G_D = 15.8$ kJ/mol) (*24*) originate to a large extent from electrostatic contributions. For *Bs*-CspB, Coulombic interactions are unfavorable, and therefore, its stability increases strongly in the presence of mono- or divalent salts. In the thermophilic protein *Bc*-Csp, the ionic interactions are strongly improved, and therefore, its stability decreases when these interactions are screened by adding 0−0.5 M NaCl (*25*).

Bs-CspB and *Bc*-Csp vary in sequence at 12 positions located at the protein surface, but the difference in stability originates from only two of them, Arg3 near the N-terminus and Leu66 at the C-terminus of *Bc*-Csp, which replace Glu3 and Glu66 of *Bs*-CspB, respectively. These two positions are close to each other in the three-dimensional structure of *Bc*-Csp (Figure 1). A thermodynamic study of multiple mutants, including a triple-mutant analysis of positions 3, 46, and 66, revealed the molecular determinants of the enhanced stability of *Bc*-Csp. The Arg3Glu difference alone accounts for approximately two-thirds of the total difference in stability and for the entire difference in the Coulombic interactions between the two proteins (*24*, *26*).

In this work, we examined how the residues at positions 3 and 66 affect the folding kinetics and asked whether the strong differences in Coulombic interactions that are so important for the stability of the folded proteins are also important for the folding process. Unlike hydrogen bonds or van der Waals interactions, Coulombic interactions are long-range and thus might control early events in folding. Our original stopped-flow analyses of the folding kinetics of the wild-type forms of *Bs*-CspB, *Bc*-Csp, and *Tm*-Csp (*23*) were performed in the presence of GdmCl, because the two thermostable proteins could not be unfolded completely by urea. The refolding rates in the absence of GdmCl had to be extrapolated from the data obtained at $\geq$0.6 M GdmCl, because at lower concentrations folding occurred in the dead time of stopped-flow mixing. The ionic denaturant GdmCl screens Coulombic interactions, and thus, their role for folding might have been obscured in these experiments.

Here we measured the folding kinetics as a function of temperature in the absence and presence of the uncharged denaturant urea by using an improved pressure-jump apparatus with a pressure range of 400 bar (40 MPa), a time resolution of 50 μs, and an operating range between 1 and 80 °C. The use of GdmCl could thus be avoided and the electrostatic contributions to the activated state of folding investigated. We find that the Coulombic interactions originating from residue 3 are indeed important for folding and are largely present already in the folding transition state of the two cold shock proteins. In contrast, the contributions of C-terminal residue 66, including its interaction with the residue at position 3, are established only late in folding.

MATERIALS AND METHODS

Materials. Urea and GdmCl (ultrapure) were from ICN (Cleveland, OH). All other chemicals were from Merck (Darmstadt, Germany). *Bc*-Csp and *Bs*-CspB were overexpressed in *E. coli* with a bacteriophage T7 RNA polymerase promotor system (*27*) and purified as described previously (*3*, *25*) with minor modifications. Protein variants were constructed by site-directed mutagenesis, overexpressed, and purified as described previously (*24*).

Heat-Induced Equilibrium Unfolding Transitions. Thermal unfolding transitions were measured in 100 mM sodium cacodylate-HCl (pH 7.0) at protein concentrations of 4 μM. The transitions were monitored by the decrease of the CD signal at 222.6 nm (1 nm bandwidth) in 1 cm cells in a JASCO J600 spectropolarimeter (JASCO, Tokyo, Japan). Heating rates were 60 °C/h. Transitions were evaluated using a nonlinear least-squares fit according to a two-state model (*28*).

Stopped-Flow Kinetic Experiments. A DX.17MV sequential mixing stopped-flow spectrometer from Applied Photophysics (Leatherhead, U.K.) was employed for all stopped-flow measurements at 25 °C. The path length of the observation chamber was 2 mm. A 10 mM aqueous solution of cytidine 2′-phosphate in a 0.5 cm cell was inserted between the observation chamber and the emission photomultiplier to absorb scattered light from the excitation beam. The folding kinetics were followed by the change in fluorescence above 300 nm after excitation at 280 nm (10 nm bandwidth).

All unfolding and refolding experiments were performed in 100 mM sodium cacodylate-HCl (pH 7.0) at 25 °C. To initiate unfolding, typically 16.5 μM native *Bc*-Csp in buffer was diluted 11-fold with GdmCl solutions of varying concentrations to give final GdmCl concentrations between 1.0 and 6.5 M. To initiate refolding, 16.5 μM unfolded *Bc*-Csp in concentrated GdmCl solutions (between 3 and 4.5 M) was diluted 11-fold with aqueous buffer or with GdmCl solutions of varying concentrations to give final concentrations of 0.3−4 M GdmCl. Kinetics were measured at least eight times under identical conditions, averaged, and analyzed as monoexponential functions by using the software provided by Applied Photophysics. The data were analyzed as described in ref *3*.

Pressure-Jump Apparatus and Experiments. On the basis of the experience with the pressure-jump apparatus described in ref *29*, an improved modular version was constructed at the Max-Planck-Institute (Dortmund, Germany). Repetitive pressure jumps are applied to the protein solution using a stack of piezoelectric crystals (*30*). The sample cell with a

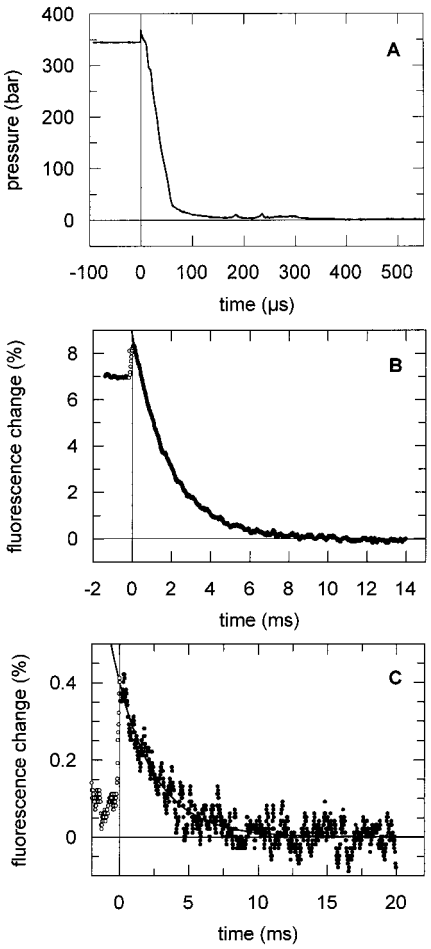

FIGURE 2: (A) Pressure profile after a jump from 350 to 3 bar. (B and C) Refolding kinetics of *Bc*-Csp R3E in 100 mM sodium cacodylate-HCl (pH 7.0) at (B) 60 °C (near the midpoint of the thermal unfolding transition) and (C) at 29 °C (in the baseline region of the native protein) following a pressure jump from 350 to 3 bar. The fluorescence above 320 nm after excitation at 280 nm was monitored. The kinetics were measured 200 times and averaged. The solid lines represent best fits to monoexponential time courses with rate constants of 525 (B) and 359 s^{-1} (C).

volume of approximately 50 μL consists of a sapphire ring, transparent in the near-UV and visible region. Optical ports in T-form allow measurements of fluorescence as well as absorption and light scattering. The crystal stack is separated from the protein solution by a thin kaptan membrane. An increased diameter of the membrane and the crystal stack piston in the new machine allows the application of larger pressures (up to 400 bar), using the PI-245.70 crystal stack (Physik Instrumente, Waldbronn, Germany). For this element, the pressure change is more than 90% complete in 100 μs with a pressure increase and in 50 μs with a pressure decrease (see Figure 2A). With the smaller PI-245.30 crystal stack, pressure changes of up to 200 bar can be applied at more than twice the speed of those with PI-245.70. Pressure is detected directly in the sample chamber using a tiny, type 6158A membrane-less sensor (Kistler, Winterthur, Switzerland). Several hundred pressure up and down jumps per minute can be performed (depending on detection time).

Fluorescence of the samples was excited at 280 nm and monitored at 90° relative to the incident light at wavelengths of >320 nm. Before each measurement, the fluorescence was adjusted to a photomultiplier output of 10 V. The folding kinetics were measured as a function of temperature, usually at 0, 2.0, 4.0, and 6.0 M urea in 100 mM sodium cacodylate-HCl (pH 7.0) at protein concentrations of 10 μM. The measurements in 1.0 M GdmCl and 1.0 M NaCl were performed in the absence of urea. For each experiment, 1−600 kinetic traces were collected, averaged, and analyzed as single-exponential functions.

Analysis of Pressure-Jump Folding Kinetics. For a two-state folding reaction (eq 1a), the equilibrium constant K_D is equal to the ratio of the microscopic rate constants for unfolding (k_{NU}) and refolding (k_{UN}) (eq 1b), and the measured rate constant λ is equal to the sum of k_{NU} and k_{UN} (eq 2).

$$\mathrm{N} \underset{k_{UN}}{\overset{k_{NU}}{\rightleftharpoons}} \mathrm{U} \tag{1a}$$

$$K_D = k_{NU}/k_{UN} \tag{1b}$$

$$\lambda = k_{NU} + k_{UN} \tag{2}$$

The Gibbs free energy of unfolding $\Delta G_D(T)$ can be calculated from the enthalpy $\Delta H_D(T)$ and the entropy $\Delta S_D(T)$ of unfolding with the Gibbs−Helmholtz equation (eq 3). In our analysis, we assume that all thermodynamic equilibrium (ΔX) and activation ($\Delta X^{\ddagger}$) parameters depend linearly on urea concentration. These dependencies are denoted as ΔX_i and $\Delta X^{\ddagger}_i$. The kinetic m value [$m = \partial(\ln k)/\partial[\mathrm{urea}]$] is equal to $-\Delta G^{\ddagger}_i/(RT)$. In all calculations, ΔC_p in the absence of urea was kept constant at a value of 4 kJ mol^{-1} K^{-1}. All heat capacity increments were also assumed to be independent of temperature. Equation 4 is taken from ref *31*. It describes the dependence on temperature and urea concentration of the two microscopic rate constants k_{NU} and k_{UN}.

$$\Delta G_D(T) = \Delta H_D(T) - T\Delta S_D(T) \tag{3}$$

$$k_{ij} = \left(\frac{k_B T}{h}\right)\left[\left(\frac{T}{T^0}\right)^{\left(\frac{\Delta C_p^{\ddagger} + \Delta C_{p,i}^{\ddagger}[\mathrm{urea}]}{R}\right)}\right] \times \exp\left[\frac{\Delta S^{\ddagger}(T^0) + \Delta S_i^{\ddagger}(T^0)[\mathrm{urea}]}{R} - \frac{\Delta H^{\ddagger}(T^0) + \Delta H_i^{\ddagger}(T^0)[\mathrm{urea}]}{RT} - \frac{(\Delta C_p^{\ddagger} + \Delta C_{p,i}^{\ddagger}[\mathrm{urea}])(T - T^0)}{RT}\right] \tag{4}$$

$$y_{obs} = \frac{y_n^0 + m_n T + (y_u^0 + m_u T)\mathrm{e}^{\left\{-\frac{\Delta H_D(T^0)}{RT} + \frac{\Delta S_D(T^0)}{R} - \frac{\Delta C_p}{R}\left[1 - \frac{T^0}{T} - \ln\left(\frac{T}{T^0}\right)\right]\right\}}}{1 + \mathrm{e}^{\left\{-\frac{\Delta H_D(T^0)}{RT} + \frac{\Delta S_D(T^0)}{R} - \frac{\Delta C_p}{R}\left[1 - \frac{T^0}{T} - \ln\left(\frac{T}{T^0}\right)\right]\right\}}} \tag{5}$$

For the individual Csp variants, the entire set of λ values derived from pressure-jump kinetics, typically measured at 0, 2.0, 4.0, and 6.0 M urea and between 1 and 80 °C (depending on denaturant concentration), together with a thermal unfolding transition in the absence of urea were subjected to a joint analysis based on the combination of eqs 1−5. In this analysis, which is based on transition state theory, we decompose the activation Gibbs free energy $\Delta G^{\ddagger}$ into its (temperature-dependent) enthalpic and entropic components, $\Delta H^{\ddagger}$ and $\Delta S^{\ddagger}$ (as in eq 3). Equation 5 describes the equilibrium unfolding transition. In this equation, y_{obs} is the observed CD signal at 222.6 nm. The CD signals of the

Table 1: Thermodynamic Parameters for the Refolding and Unfolding of *Bc*-Csp, *Bs*-CspB, and Variants[a]

	k_{UN} (s^{-1})	k_{NU} (s^{-1})	ΔG_D (kJ/mol)	$\Delta\Delta G_D$ (kJ/mol)	$\Delta\Delta G^{\ddagger}_{UN}$ (kJ/mol)	$\Delta\Delta G^{\ddagger}_{NU}$ (kJ/mol)	Φ_{UN}	m_{UN} (M^{-1})	m_{NU} (M^{-1})	α
Bc-Csp	2253	462	4.5	–	–	–	–	−0.71	0.07	0.91
Bs-CspB	253	9938	−10.5	−15.0	6.2	−8.8	0.42	−0.44	−0.09	1.26
Bc-Csp Q2L	5971	542	6.8	2.3	−2.8	−0.5	1.20	−0.79	0.07	0.92
Bc-Csp R3E	124	1217	−6.5	−11.0	8.3	−2.8	0.75	−1.34	0.01	0.99
Bc-Csp N11S	3530	450	5.9	1.4	−1.3	0.1	0.95	−0.84	0.09	0.90
Bc-Csp Y15F	2003	447	4.3	−0.2	0.3	0.1	–	−0.85	0.11	0.89
Bc-Csp G23Q	1109	358	3.2	−1.3	2.0	0.7	1.57	−0.73	0.13	0.84
Bc-Csp S24D	2422	364	5.4	0.9	−0.2	0.7	–	−0.79	0.10	0.89
Bc-Csp T31S	2491	418	5.1	0.6	−0.3	0.3	–	−0.84	0.10	0.89
Bc-Csp E46A	1277	385	3.4	−1.1	1.6	0.5	1.48	−0.88	0.06	0.94
Bc-Csp Q53E	2250	572	3.9	−0.6	0	−0.6	–	−0.68	0.05	0.93
Bc-Csp V64T	2041	642	3.3	−1.2	0.3	−0.9	0.23	−0.91	0.11	0.89
Bc-Csp L66E	1575	1997	−0.7	−5.2	1.0	−4.2	0.20	−0.69	0.04	0.94
Bc-Csp 67A	2520	512	4.5	0	−0.3	−0.3	–	−0.71	0.09	0.89
Bc-Csp R3L	933	745	0.6	−3.9	2.5	−1.4	0.65	−0.79	0.01	0.99
Bc-Csp R3E/E46A	234	730	−3.3	−7.8	6.5	−1.3	0.83	−0.78	0.04	0.94
Bc-Csp R3E/L66E	55	14581	−15.9	−20.4	10.6	−9.8	0.52	0.85	−0.04	0.95
Bc-Csp E46A/L66E	789	1156	−1.1	−5.6	3.0	−2.6	0.53	−1.06	−0.02	1.03
Bc-Csp R3E/E46A/L66E	94	6771	−12.2	−16.7	9.1	−7.7	0.54	−0.99	−0.04	1.04
Bs-CspB E3R	1434	1538	−0.2	10.3	−5.0	5.3	0.48	−0.60	0.08	0.88
Bs-CspB E66L	488	1050	−2.2	8.3	−1.9	6.4	0.23	−0.84	0.10	0.89
Bs-CspB E3R/E66L	2115	759	2.9	13.4	−6.1	7.3	0.45	−0.78	0.09	0.90

[a] The thermodynamic activation parameters for refolding and unfolding are denoted by the subscripts UN and NU, respectively. All kinetics were measured in 100 mM sodium cacodylate-HCl (pH 7.0) at 70 °C after pressure jumps. Measurements were performed and data analyzed as described in the legend of Figure 3. k_{UN} and k_{NU} are the microscopic rate constants of refolding and unfolding, respectively, in the absence of denaturant. ΔG_D is the equilibrium Gibbs free energy of unfolding in the absence of urea. $\Delta\Delta G_D$ is the difference in ΔG_D between *Bs*-CspB and *Bc*-Csp or between the variant and the respective wild-type protein (*Bc*-Csp or *Bs*-CspB). $\Delta\Delta G^{\ddagger}$ is the difference in $\Delta G^{\ddagger}$ between the variant and the respective wild-type protein. Φ_{UN} is the ratio of $-\Delta\Delta G^{\ddagger}_{UN}$ and $\Delta\Delta G_D$. Φ_{UN} values derived from $\Delta\Delta G_D$ values of <1 kJ/mol are not given. m is the dependence on urea concentration of $\Delta G^{\ddagger}$ $\{[\partial(\Delta G^{\ddagger})]/(\partial[\text{urea}])\}$ over $-RT$. α is the fractional change of the m value during refolding $[=m_{UN}/(m_{UN} - m_{NU})]$.

folded and unfolded forms y_n and y_u, respectively, are assumed to vary linearly with temperature with slopes m_n and m_u, respectively. y_n^0 and y_u^0 are identical with y_n and y_u at 0 K, respectively.

Analysis of Interaction Energies in the Triple-Mutant Cube. Interaction energies between the amino acid side chains of Glu3, Glu46, and Glu66 were determined by construction of a triple-mutant cube as described in refs *26* and *32*. $\Delta\Delta G$ values smaller than zero refer to repulsion energies. $\Delta\Delta G_{eq}$ is the equilibrium interaction energy calculated from the ΔG_D values in Table 1. $\Delta\Delta G^{\ddagger}_{UN}$ describes the energetic coupling of the activation energies of refolding $\Delta G^{\ddagger}_{UN}$ (Table 1) multiplied by −1, and thus accounts for the interaction energy already present in the transition state for refolding. $\Delta\Delta G^{\ddagger}_{NU}$ is the interaction energy established after the passage through the folding transition state. It is calculated from the activation energies of unfolding $\Delta G^{\ddagger}_{NU}$ in Table 1.

RESULTS

Pressure-Induced Folding Kinetics of the Cold Shock Protein. We determined the microscopic rate constants of unfolding and refolding from the apparent rate constant λ and the equilibrium constant K_D (eqs 1 and 2) as a function of temperature and urea concentration. The kinetics of folding were measured after pressure jumps, and the equilibrium constants were derived from thermal unfolding transitions. In our previous work, the magnitude of the pressure jumps (Δp) was confined to ≤160 bar (16 MPa). With the improved version of the pressure-jump apparatus, the pressure range could be extended to ≤400 bar without compromising the excellent time resolution. The pressure profile for a jump from 350 to 3 bar with the new apparatus is shown in Figure 2A. Approximately 90% of the pressure decrease occurs in a linear fashion within 50 μs, which allows rate constants of more than 10 000 s^{-1} to be determined with high precision. The corresponding pressure up jumps from 3 to 350 bar show nearly the same time resolution (100 μs). After the jumps, the final pressure remains stable for more than 100 s, and thus, a reaction can be followed in the time range from microseconds to minutes in a single experiment.

We measured rate constants of folding after both pressure up and pressure down jumps, but only the pressure down jumps are used for the analysis because here folding occurs near ambient pressure and can be combined with the equilibrium data to calculate the microscopic rate constants. The activation volumes are positive for both unfolding and refolding (*29*) of the cold shock proteins, and therefore, folding becomes slower with increasing pressure.

The amplitudes of refolding are highest near the transition midpoint. This is illustrated by the refolding reaction of the Arg3Glu variant of *Bc*-Csp at 60 °C after a jump from 350 to 3 bar (Figure 2B). Under these conditions, the amplitude of refolding reaches 9% of the final value. With the improved pressure-jump apparatus, the folding kinetics can be measured even under conditions where the [N]/[U] ratio is near 200. Here the change in fluorescence after a jump from 350 to 3 bar is only ∼0.4%. Nevertheless, as shown for the refolding of *Bc*-Csp R3E at 29 °C (Figure 2C), repetitive measurements and averaging allow the rate of folding to be determined even under these conditions, which strongly favor the native protein.

Folding Kinetics of Bs-CspB over a Wide Range of Temperature. The wild-type form of *Bs*-CspB exhibits a low

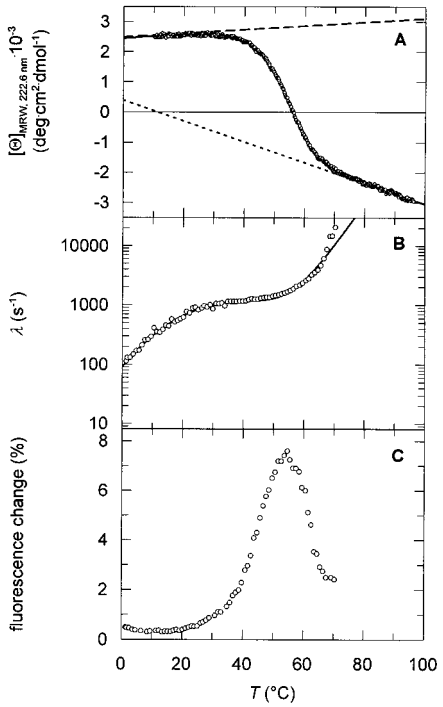

FIGURE 3: (A) Thermal unfolding transition of *Bs*-CspB. (B) Apparent rate constants λ and (C) amplitudes of refolding derived from pressure-jump experiments for *Bs*-CspB. All measurements were performed in 100 mM sodium cacodylate-HCl (pH 7.0). The lines in panels A and B represent the results of the combined analysis of equilibrium and kinetic data based on eqs 1−5. In panel A, the baselines of the native and the unfolded protein are shown as dashed and dotted lines, respectively. The amplitudes in panel C are given as a percentage of the final value.

thermodynamic stability. Its thermal unfolding transition (Figure 3A, $T_M = 53.6$ °C) is broad because the enthalpy of denaturation ΔH_D is small and becomes zero near 5 °C. As a consequence, ΔG_D reaches a broad maximum of ∼12 kJ/mol, and the [N]/[U] ratio shows an almost constant value of ∼200 between 0 and 15 °C. As indicated in Figure 2C, a 350 to 3 bar jump shifts the folding equilibrium sufficiently enough to allow the kinetics to be determined under these conditions, which, apparently, are equivalent to the baseline kinetics for the folded protein in the transition shown in Figure 3A. The folding kinetics of *Bs*-CspB could thus be determined over a very broad range of temperature between 1 and 70 °C. The measured rate constants λ (Figure 3B) increase from 100 s^{-1} at 1 °C to ∼20000 s^{-1} at 70 °C. The corresponding amplitudes (Figure 3C) show a bell-shaped dependence on temperature with a maximum near the transition midpoint.

The kinetic and equilibrium data in panels A and B of Figure 3 were analyzed, together with kinetics measured in the presence of 2.0, 4.0, and 6.0 M urea (cf. eqs 1−5). The resulting microscopic rate constants and activation parameters are listed in Table 1. The calculated temperature dependence of λ is shown by the continuous line in Figure 3B. λ reflects the rate constant of refolding (k_{UN}) at low temperatures and the rate constant of unfolding (k_{NU}) at high temperatures. The downward curvature at low temperatures is caused by the negative activation heat capacity of refolding, which renders the activation enthalpy of refolding negative above ∼36 °C. In the region of the equilibrium transition (between 37 and 67 °C), the slope of the curve increases again because

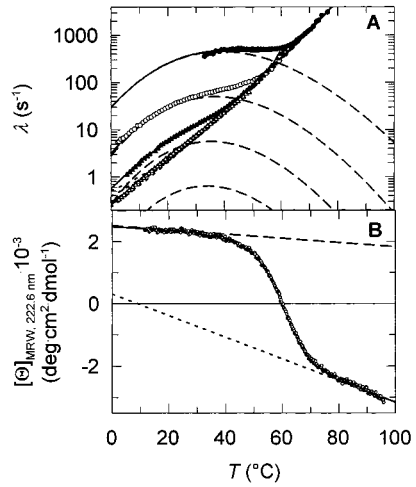

FIGURE 4: (A) Apparent rate constants λ of folding for *Bc*-Csp R3E in 0 (●), 2 (○), 4 (▲), and 6 M urea (△). The data were derived from pressure-jump experiments in 100 mM sodium cacodylate-HCl (pH 7.0). The solid lines represent nonlinear least-squares fits of the kinetic data and the thermal unfolding transition in panel B according to eqs 1−5. The calculated profiles for k_{NU} (dotted lines) and k_{UN} (dashed lines) are shown for the measured urea concentrations. The profiles for k_{NU} largely coincide with the λ values measured at 6.0 M urea. (B) Thermal unfolding transition of *Bc*-Csp R3E in 100 mM sodium cacodylate-HCl (pH 7.0). The fit result is shown as a solid line, and the baselines for the native and the unfolded protein are shown as dashed and dotted lines, respectively.

the value of λ approaches the rate of unfolding (k_{NU}), which is correlated with a high positive activation enthalpy.

The temperature range that is accessible for pressure-jump measurements is narrower for the variants of the cold shock protein with enhanced stability, because ΔH_D increases with temperature, and therefore, K_D changes more strongly with temperature. This is illustrated in Figure 4 for *Bc*-Csp R3E, the folding kinetics of which could be measured between 30 and 77 °C. To extend the accessible temperature range, urea was added to the solvent. Urea shifts the thermal unfolding transition to lower temperatures and decreases its cooperativity. Pressure-jump data obtained in the presence of 2.0, 4.0, and 6.0 M urea are also shown in Figure 4A. In combination, these data cover the temperature range between 1 and 77 °C, which is essentially identical with the operating range of the pressure-jump apparatus. In 6.0 M urea, the unfolded form of the protein predominates at all temperatures, and therefore, the measured λ values give direct information about k_{NU} and its dependence on temperature. Figure 4A also indicates that k_{NU} is almost independent of the urea concentration, as expected from previous data (*31*).

For the two wild-type proteins *Bs*-CspB and *Bc*-Csp and for most of the variants, we measured the folding kinetics as a function of temperature in 1 °C intervals in the presence of 0, 2.0, 4.0, and 6.0 M urea in 100 mM sodium cacodylate-HCl (pH 7.0). All kinetics could be represented by single-exponential functions, confirming the two-state character of folding in the range of temperature and denaturant concentrations of this study. Usually, an entire temperature profile was collected with a single filling of the pressure cell. Control experiments with fresh samples at high temperatures gave identical rate constants. In some cases, small differences in the amplitudes were observed.

To determine the kinetic activation parameters $\Delta H^{\ddagger}$, $\Delta S^{\ddagger}$, and $\Delta C_p^{\ddagger}$ for unfolding and refolding (cf. eqs 1−5), the

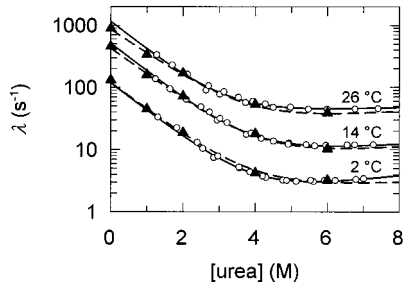

FIGURE 5: Comparison of pressure-jump (▲) and stopped-flow (○) data for the folding of *Bs*-CspB [in 100 mM sodium cacodylate-HCl (pH 7.0)] as a function of urea concentration at 2, 14, and 26 °C. The stopped-flow data are taken from ref *31*. The fit results for these data are shown as solid lines, and the fit results for the pressure-jump data are shown as dashed lines.

kinetic data obtained as a function of temperature in 0−6 M urea were combined with the stability data measured in the absence of urea. The pressure-jump measurements cover a wide temperature range, suggesting that the activation heat capacities $\Delta C_p^{\ddagger}$ can be estimated as well. Still, the $\Delta C_p^{\ddagger}$ values are derived from the second derivative of the rate constants, and therefore, to improve reliability, the equilibrium ΔC_p was kept constant at 4 kJ mol^{-1} K^{-1}, which represents the average of the ΔC_p values from the thermal unfolding transitions. Table 1 gives the values for the activation Gibbs free energies ($\Delta G^{\ddagger}$) at 70 °C, which is within the transition region for most variants. Here the apparent rate constants and the equilibrium stability could be measured with high precision, and thus, the calculated $\Delta G^{\ddagger}$ values are reliable.

The folding reactions of the cold shock proteins are diffusional reactions and depend on solvent viscosity (*33*−*35*). The temperature and denaturant concentration-dependent changes in solvent viscosity, however, hardly affect the activation and equilibrium Gibbs free energies in the absence of denaturant (*36*), and therefore, a correction for viscosity effects was not made. Moreover, these small effects cancel out when $\Delta\Delta G^{\ddagger}$ values are calculated. Figure 4 shows the results of the joint analysis of the kinetic and equilibrium data for *Bc*-Csp R3E, and the respective parameters for all variants are given in Table 1.

Comparison of Pressure-Jump and Stopped-Flow Data. The folding kinetics of wild-type *Bs*-CspB have been measured previously as a function of urea concentration (0−8 M) between 2 and 45 °C after stopped-flow mixing (*31*). Figure 5 compares these data with the λ values obtained from the pressure-jump measurements. The two sets of data and their analyses coincide very well. Due to the excellent time resolution and the high sensitivity of the improved pressure-jump apparatus, the folding kinetics of *Bs*-CspB at 0 M urea could by measured directly (cf. Figure 3). These measured values agree very well with the values that were obtained previously by a linear extrapolation of the stopped-flow data (Figure 5). This suggests that this linear extrapolation is indeed valid for *Bs*-CspB using urea as the denaturant and excludes a "rollover" in the refolding kinetics at low denaturant concentrations, conditions under which folding is complete within the dead time of stopped-flow mixing. The two methods for measuring the folding kinetics complement each other very well. Stopped-flow experiments can be carried out under strongly unfolding conditions, which, for lack of amplitude, cannot be explored in pressure-jump experiments. Pressure-jump experiments, on the other hand, can be performed at much higher temperatures and in the absence of a denaturant, and their time resolution is at least 20-fold higher.

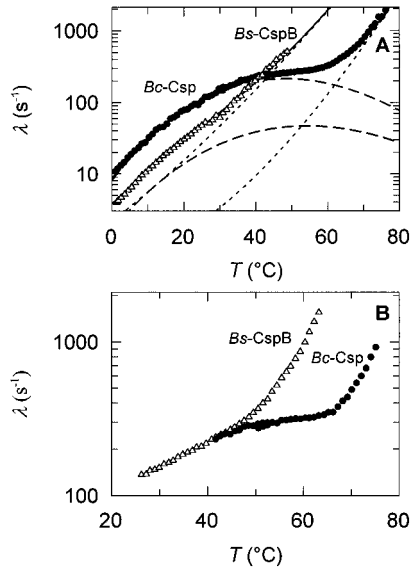

FIGURE 6: Apparent rate constants λ of refolding derived from pressure-jump experiments for *Bc*-Csp (●) and *Bs*-CspB (Δ) in (A) 4.0 M urea and (B) 1.0 M GdmCl, 1.0 M NaCl, and 100 mM sodium cacodylate-HCl (pH 7.0). The lines in panel A represent the results of the combined analysis of equilibrium and kinetic data based on eqs 1−5.

Pressure-Jump-Induced Folding Kinetics of Wild-Type Bc-Csp. The stopped-flow investigation of the folding kinetics of the thermophilic cold shock proteins *Bc*-Csp and *Tm*-Csp required the use of GdmCl as the denaturant, because these proteins could not be unfolded completely by urea at ambient temperature (*23*). It is now clear that electrostatic interactions contribute strongly to the enhanced stability of *Bc*-Csp (*24*). GdmCl screens these interactions, and thus, their contributions to the stabilization of the folding transition state could not be derived from folding experiments in the presence of GdmCl. The pressure-jump apparatus operates up to 80 °C, a temperature beyond the midpoint of the thermal unfolding transition of *Bc*-Csp, and therefore, the rate constants of both unfolding and refolding could be determined in the absence of GdmCl.

The folding kinetics of wild-type *Bc*-Csp were measured by the pressure-jump technique between 1 and 80 °C in the presence of 0, 2.0, 4.0, and 6.0 M urea. Figure 6A compares the kinetics obtained in 4.0 M urea with the corresponding folding kinetics of *Bs*-CspB. At 70 °C in 100 mM buffer and in the absence of salt, the two proteins differ in stability by 15.8 kJ/mol (*24*). Figure 6A shows that this difference originates from a 22-fold decrease in the unfolding rate ($\Delta\Delta G^{\ddagger}_{NU} = 8.8$ kJ/mol) and a 9-fold increase in the rate of refolding ($\Delta\Delta G^{\ddagger}_{UN} = -6.2$ kJ/mol) of *Bc*-Csp (Table 1).

Our previous stopped-flow kinetic measurements in the presence of GdmCl had suggested that the increased thermostability of *Bc*-Csp is mainly a consequence of a reduced rate of unfolding ($\Delta\Delta G^{\ddagger}_{NU} = 6.9$ kJ/mol); the refolding rate was almost unchanged ($\Delta\Delta G^{\ddagger}_{UN} = -1.7$ kJ/mol) (*23*) (Table 3). The difference in the activation data measured in the absence of GdmCl (Figure 6A) thus suggests that the ionic

Table 2: Thermodynamic Parameters for the Refolding and Unfolding of *Bc*-Csp, *Bs*-CspB, and *Bc*-Csp R3L in 1.0 M GdmCl and 1.0 M NaCl[a]

	k_{UN} (s^{-1})	k_{NU} (s^{-1})	ΔG_D (kJ/mol)	$\Delta\Delta G_D$ (kJ/mol)	$\Delta\Delta G^{\ddagger}_{UN}$ (kJ/mol)	$\Delta\Delta G^{\ddagger}_{NU}$ (kJ/mol)
Bc-Csp	259	38	5.2	–	–	–
Bs-CspB	119	426	−3.5	−8.7	2.1	−6.6
Bc-Csp R3L	262	40	5.2	0	−0.1	−0.1

[a] Thermodynamic parameters are derived from pressure-jump measurements in 1.0 M GdmCl, 1.0 M NaCl, and 100 mM sodium cacodylate-HCl (pH 7.0). They are given for 55 °C. Parameters are defined as described in the footnote of Table 1.

interactions, which are screened in GdmCl solutions, primarily affect refolding and are largely established in the activated state of folding already.

The stopped-flow experiments were performed at 25 °C, but the pressure-jump data are calculated for a temperature of 70 °C. To examine whether the observed differences in the activation parameters reflect a temperature-dependent shift of the transition state, rather than a salt effect, we performed pressure-jump experiments in the presence of a mixture of 1.0 M NaCl and 1.0 M GdmCl, conditions under which *Bs*-CspB and *Bc*-Csp differ in stability by only 8.7 kJ/mol (at 55 °C). The stability difference under these conditions is thus nearly the same as in 2.0 M NaCl at 70 °C (*24*) or in 2 M GdmCl at 25 °C (*23*). The combination of 1.0 M NaCl and 1.0 M GdmCl was chosen because both proteins are destabilized to a moderate extent and thus pressure-jump measurements could be performed over a broad temperature range. At low temperatures, *Bs*-CspB and *Bc*-Csp exhibit almost identical rates of refolding (Figure 6B); they differ, however, strongly at high temperatures where λ approaches the rate of unfolding. The analysis (Table 2) results in activation energies for refolding ($\Delta\Delta G^{\ddagger}_{UN} = -2.1$ kJ/mol at 55 °C) and unfolding ($\Delta\Delta G^{\ddagger}_{NU} = 6.6$ kJ/mol at 55 °C) that are almost identical with the values calculated from the kinetics in GdmCl. This confirms that the differences observed originally between the stopped-flow and pressure-jump measurements reflect the salt effect of GdmCl on the folding transition state. A major fraction of the Coulombic interactions that contribute to the additional stability of *Bc*-Csp appear to be present in the folding transition state already. Screening by salt abolishes these interactions and thus decreases the difference in the refolding barrier between *Bc*-Csp and *Bs*-CspB by ~4 kJ/mol.

Contributions of Individual Sequence Differences to the Stability of the Folding Transition State. The 10 sequence differences between *Bc*-Csp and *Bs*-CspB that had little influence on equilibrium stability (*24*) also exerted little influence on the folding kinetics (Figure 7A). The respective mutants differed from wild-type *Bc*-Csp by less than 1 kJ/mol in $\Delta G^{\ddagger}_{NU}$ and by ≤2 kJ/mol in $\Delta G^{\ddagger}_{UN}$ (Table 1). Only the Gln2Leu mutation had a significant accelerating effect on refolding. These variants differ also very little from the folding kinetics of the wild-type protein when stopped-flow data at 25 °C are compared (Figure 9A).

The Leu66Glu mutation destabilizes *Bc*-Csp by 5.2 kJ/mol, which originates predominantly from a 4-fold increase in the rate of unfolding ($\Delta\Delta G^{\ddagger}_{NU} = 4.2$ kJ/mol) (Figure 7B and Table 1). The corresponding Φ_{UN} value is 0.20, which suggests that the additional stabilization of folded *Bc*-Csp by Leu66 (relative to Glu66 of *Bs*-CspB) is established to a small extent only in the folding transition state. The Φ_{UN} value for the adjacent Val64Thr substitution shows a similar value (0.23, Table 1).

The Arg3Glu difference accounts for ~70% of the difference in the thermodynamic stability between *Bs*-CspB and *Bc*-Csp (*24*). The corresponding Arg3Glu mutation in *Bc*-Csp predominantly affects the refolding kinetics (Figure 7B). $\Delta G^{\ddagger}_{UN}$ is increased by 8.3 kJ/mol and $\Delta G^{\ddagger}_{NU}$ decreased by 2.8 kJ/mol (Table 1), leading to a Φ_{UN} value of 0.75. This suggests that the stabilization by Arg3 (relative to Glu3) is largely established in the transition state of folding already. *Bc*-Csp R3E thus refolds 18 times slower than the wild-type protein and even 2 times slower than *Bs*-CspB. The Gln → Leu mutation at the adjacent position 2 shows a similar result. It stabilizes *Bc*-Csp by a 2.5-fold increase in the rate of refolding (Table 1), which overcompensates for a 1.2-fold increase in the rate of unfolding, leading to a Φ_{UN} of 1.20. Together, these results indicate that on the folding pathway N-terminal residues 2 and 3 are ordered already in the transition state, whereas residues 64 and 66 at the C-terminus are engaged to a small extent only in their native interactions.

Role of Electrostatic Surface Interactions in the Transition State. Pairs of Glu residues at positions 3 and 66 or at positions 3 and 46 destabilize *Bs*-CspB by pairwise Coulombic repulsions, which decrease ΔG_D by 4 kJ/mol each. This was shown by a triple-mutant analysis in which the residues at positions 3, 46, and 66, as they occur in *Bs*-CspB and *Bc*-Csp, were combined in all possible manners in variants of *Bc*-Csp (*26, 32*). Interactions between residues 46 and 66 could not be found in this analysis. We now asked how these unfavorable electrostatic interactions affect the transition state of folding. To this end, we measured the folding kinetics of the eight variants that constitute the triple-mutant cycle.

The results of this analysis are shown in Figure 8. As in the equilibrium experiments, we find virtually no coupling between Glu46 and Glu66 at the level of the activation energies, which suggests that these two Glu residues interact neither in the activated state of folding nor in the native protein.

The unfavorable Glu3−Glu46 and Glu3−Glu66 repulsions are established to different extents in the time course of folding. The Glu3−Glu46 repulsion is already ~75% and the Glu3−Glu66 repulsion only ~25% established in the folding transition state (Figure 8). Together with the individual Φ_{UN} values of the N- and C-terminal residues (Table 1), these results indicate that the N-terminal region is largely nativelike, including its interaction with position 46, in the folding transition state, whereas the C-terminal residues establish their nativelike interactions predominantly after passage through the transition state.

Not only does Arg3 stabilize *Bc*-Csp by removing 4 kJ/mol of unfavorable Coulombic interaction energy, but its positively charged guanidinium group also contributes 3 kJ/mol of general electrostatic stabilization. Accordingly, when the positive charge is abolished, as in the *Bc*-Csp R3L variant, the protein loses 3.9 kJ/mol in stability; 2.5 kJ/mol of this loss is accounted for by changes between the unfolded and the transition state and 1.4 kJ/mol by changes between the transition state and the native state (Table 1). These differences vanish in high salt, and the folding kinetics of

Table 3: Thermodynamic Parameters for the Refolding and Unfolding of *Bc*-Csp, *Bs*-CspB, and Variants As Derived from Stopped-Flow Measurements in the Presence of GdmCl[a]

	k_{UN} (s^{-1})	k_{NU} (s^{-1})	$[GdmCl]_M$ (M)	ΔG_D (kJ/mol)	$\Delta\Delta G_D$ (kJ/mol)	$\Delta\Delta G^{\ddagger}_{UN}$ (kJ/mol)	$\Delta\Delta G^{\ddagger}_{NU}$ (kJ/mol)	Φ_{UN}	m_{UN} (M^{-1})	m_{NU} (M^{-1})	α
Bc-Csp	1370	0.64	2.57	19.0	–		–	–	−2.76	0.22	0.92
Bs-CspB	688	9.93	1.37	10.5	−8.5	1.7	−6.9	0.20	−2.82	0.27	0.91
Bc-Csp Q2L	1626	0.67	2.90	19.3	0.3	−0.4	−0.2	–	−2.40	0.29	0.89
Bc-Csp R3E	288	0.58	2.21	15.4	−3.6	3.9	0.2	1.07	−2.57	0.24	0.92
Bc-Csp N11S	1111	0.71	2.63	18.3	−0.7	0.5	−0.3	–	−2.53	0.27	0.90
Bc-Csp Y15F	661	0.55	2.61	17.6	−1.4	1.8	0.3	1.26	−2.46	0.26	0.90
Bc-Csp G23Q	496	0.45	2.50	17.4	−1.6	2.5	0.8	1.52	−2.53	0.27	0.90
Bc-Csp S24D	900	0.45	2.73	18.9	−0.1	1.1	0.8	–	−2.48	0.30	0.89
Bc-Csp T31S	923	0.53	2.62	18.5	−0.5	1.0	0.4	–	−2.58	0.27	0.90
Bc-Csp E46A	1090	0.59	2.44	18.6	−0.4	0.6	0.1	–	−2.87	0.21	0.93
Bc-Csp Q53E	940	0.71	2.56	17.8	−1.2	1.0	−0.3	0.76	−2.59	0.22	0.92
Bc-Csp V64T	757	0.99	2.33	16.5	−2.5	1.5	−1.1	0.57	−2.54	0.31	0.89
Bc-Csp L66E	668	2.85	2.01	13.5	−5.5	1.8	−3.8	0.32	−2.60	0.12	0.96
Bc-Csp 67A	829	0.84	2.50	17.1	−1.9	1.3	−0.7	0.64	−2.55	0.22	0.92

[a] The thermodynamic parameters of refolding (UN) and unfolding (NU) for *Bc*-Csp, *Bs*-CspB, and protein variants are derived from stopped-flow measurements at 25 °C in 100 mM sodium cacodylate-HCl (pH 7.0). $[GdmCl]_M$ is the GdmCl concentration at which $K_D = 1$. m_{UN} and m_{NU} are the dependencies of ln k_{UN} and ln k_{NU} on GdmCl concentration, respectively. The other parameters are defined in the footnote of Table 1. Data for *Bc*-Csp and *Bs*-CspB are taken from ref *23*.

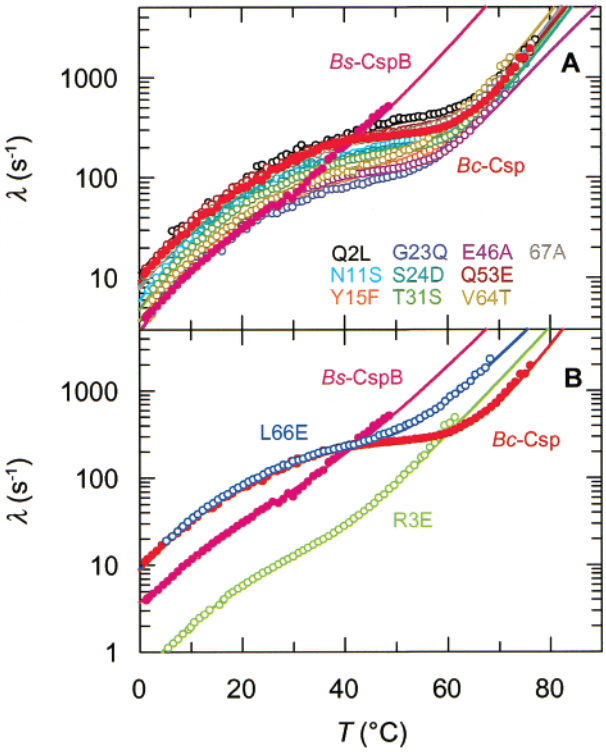

FIGURE 7: Apparent rate constants λ of refolding derived from pressure-jump experiments for *Bc*-Csp, *Bs*-CspB, and *Bc*-Csp variants in 4.0 M urea and 100 mM sodium cacodylate-HCl (pH 7.0). The lines represent the results of the combined analysis of equilibrium and kinetic data based on eqs 1−5 (Table 1). In panel A, variants with folding kinetics similar to those of the wild-type protein are shown. Panel B shows the variants with a strong influence on the folding kinetics.

wild-type *Bc*-Csp and the Arg3Leu variant become identical (Table 2). These results virtually complete the evidence that the electrostatic interactions of the charged residues at position 3 strongly influence the refolding of the two cold shock proteins, and that they are to a large extent established already when the transition state is reached.

The Leu66Glu substitution destabilizes *Bc*-Csp by nonpolar effects, which are insensitive to salt (*24*). Accordingly, the analysis of the folding kinetics of *Bc*-Csp L66E measured by stopped-flow experiments at 25 °C as a function of GdmCl concentration (Figure 9B and Table 3) gave activation parameters ($\Delta\Delta G^{\ddagger}_{UN} = 1.8$ kJ/mol, $\Delta\Delta G^{\ddagger}_{NU} = -3.8$ kJ/mol) that are very similar to the values derived from the temperature-dependent pressure-jump measurements ($\Delta\Delta G^{\ddagger}_{UN} = 1.0$ kJ/mol, $\Delta\Delta G^{\ddagger}_{NU} = -4.2$ kJ/mol) at 70 °C.

The $\Delta\Delta G_D$ between wild-type *Bc*-Csp and the Arg3Glu mutant decreases from 11.5 to 4.2 kJ/mol when 2 M NaCl is added (*24*) and to 3.6 kJ/mol when the GdmCl-induced kinetics are compared (Table 3). This suggests that ∼4 kJ/mol of the stability difference is of nonionic, presumably hydrophobic origin. This contribution seems to be present in the folding transition state of *Bc*-Csp already, because the GdmCl-dependent folding kinetics of the Arg3Glu variant and the wild-type protein (Figure 9B) differ only in refolding. $\Delta\Delta G^{\ddagger}_{UN} = 3.9$ kJ/mol (Table 3), and the resulting Φ_{UN} value is 1.07. This indicates that the nonionic interactions of Arg3 are established in the transition state of folding as well.

Conservation of the Folding Transition State of Cold Shock Proteins. The folding transition states of the wild-type forms of *Bs*-CspB and *Bc*-Csp resemble each other in their thermodynamic properties, such as enthalpy, entropy, and heat capacity (*36*), as well as in their overall nativelike interactions with denaturants, as derived from the analysis of the *m* values of unfolding and refolding (*23*). We have now probed the role of individual residue positions for folding by comparing the effects of reciprocal mutations at individual sites in the two proteins.

The substitutions Leu66Glu in *Bc*-Csp and Glu66Leu in *Bs*-CspB yield almost identical values for Φ_{UN} (0.20 and 0.23, respectively; Table 1). This Glu ↔ Leu exchange adds or deletes the nonpolar interactions of the Leu residue, but in the *Bs*-CspB background, it also removes the electrostatic repulsion between Glu3 and Glu66, which destabilizes the wild-type protein by 4 kJ/mol (*26*, *32*). This repulsion is correlated with a Φ_{UN} of 0.2 (cf. the triple-mutant analysis in Figure 8), which agrees well with the observed overall Φ_{UN} of 0.23 for the Glu66Leu mutation of *Bs*-CspB.

The Arg3Glu exchange at position 3 yields Φ_{UN} values of 0.48 and 0.75 in the *Bs*-CspB and *Bc*-Csp backgrounds, respectively. This is explained by the results of the triple-

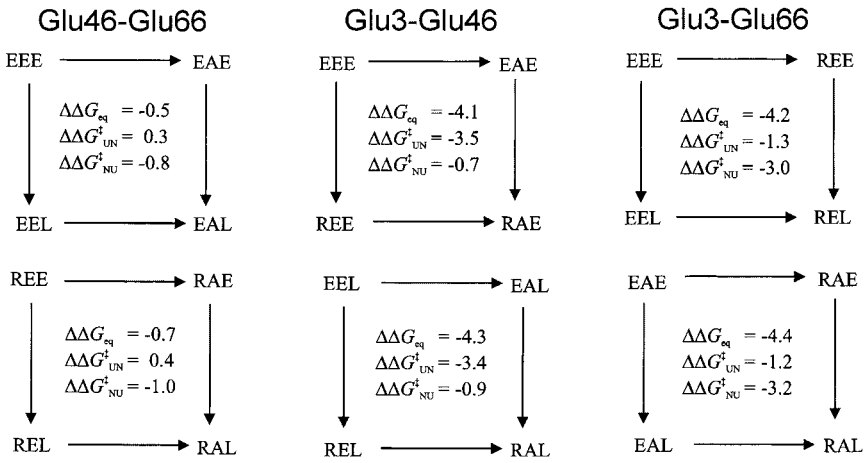

FIGURE 8: Analysis of the folding kinetics by double-mutant cycles to assess interactions among residues Glu3, Glu46, and Glu66 in the folding transition state at 70 °C. Variants are named after the amino acids at these positions. The single-letter notation for amino acids is used. $\Delta\Delta G_{eq}$ is the interaction energy derived from the equilibrium free energies of unfolding ΔG_D of the joint fit of the kinetic and equilibrium data (Table 1). $\Delta\Delta G^{\ddagger}_{UN}$ was calculated from the free energies between the unfolded and transition state, and $\Delta\Delta G^{\ddagger}_{NU}$ was calculated from the free energies between the transition and folded state in the absence of urea.

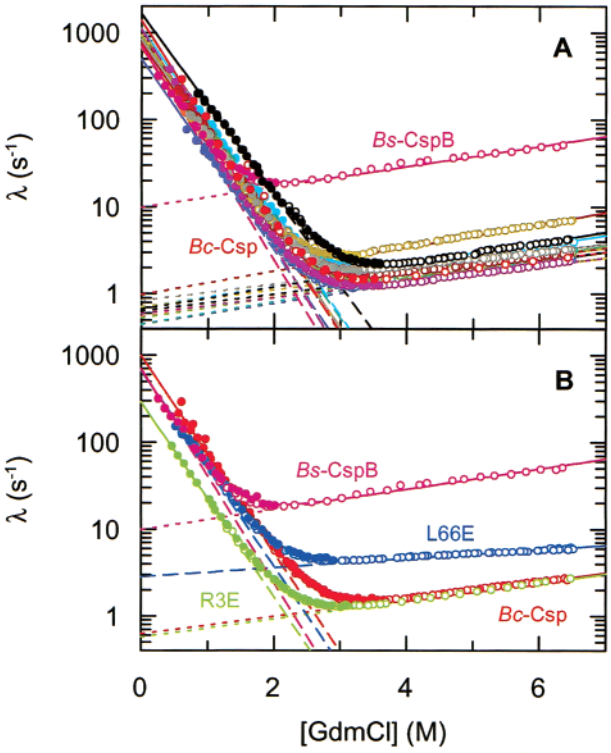

FIGURE 9: (A and B) Kinetics of unfolding (○) and refolding (●) of *Bc*-Csp, *Bs*-CspB, and *Bc*-Csp variants at 25 °C in 100 mM sodium cacodylate-HCl (pH 7.0), as derived from stopped-flow measurements. The apparent rate constant λ is shown as a function of the GdmCl concentration. Fits of the data on the basis of a linear two-state model are shown as solid lines (Table 3). The dashed and dotted lines represent the computed dependencies on GdmCl concentration of the microscopic rate constants of unfolding and refolding, k_{NU} and k_{UN}, respectively, for the proteins. The variants in panel A are color-coded as in Figure 7A.

mutant cube (Figure 8). The repulsion between Glu3 and Glu46, which occurs only in *Bc*-Csp R3E, is largely present in the transition state already, in contrast to the repulsion between Glu3 and Glu66, which contributes to folding of *Bs*-CspB.

Wild-type *Bs*-CspB refolds 9-fold slower than *Bc*-Csp. This difference originates largely from the nature of the amino acid at position 3. The stabilized variant *Bs*-CspB E3R refolds only 1.6-fold slower than *Bc*-Csp; the Glu3Arg/Glu66Leu double mutant of *Bs*-CspB, which has the same residues as *Bc*-Csp at positions 3 and 66, refolds at the same rate as *Bc*-Csp (Table 1). This suggests that the two proteins show very similar folding transition states, and that the residue at position 3 with its high Φ_{UN} value and its distinct electrostatic interactions is largely responsible for the differences in the refolding rates of the various Csp variants. This is further highlighted by the Arg3Glu mutation that decelerates the refolding of *Bc*-Csp 18-fold (Table 1). All mutations of this study left the overall strongly nativelike character of the transitions state unchanged. The α values are in the range of 0.9 (Tables 1 and 3) for all protein variants of *Bc*-Csp and *Bs*-CspB.

DISCUSSION

Pressure Jumps To Follow Protein Folding. With the improved pressure-jump apparatus, pressure changes of ±400 bar can be accomplished within ~50 μs. The sensitivity of the instrument is high enough to measure the folding kinetics within the thermal unfolding transition in a range where the [N]/[U] ratio changes from 200 to 0.02. The accessible range is particularly broad for proteins with a low stability and a low enthalpy of unfolding, such as *Bs*-CspB. In favorable cases, the folding kinetics can be measured across the region of maximal stability to the onset of cold unfolding until the lower limit of the operating range of the instrument (currently near 1 °C) is reached. This region is inaccessible by temperature-jump experiments, because the unfolding enthalpy, but not the unfolding volume, is close to zero under these conditions. For proteins with high stability (such as *Bc*-Csp), the temperature range can be extended by adding urea, which decreases both the protein stability and the apparent enthalpy of unfolding (*37*) and thus increases the temperature of maximal stability.

Contribution of the Chain Termini to the Folding Kinetics of the Cold Shock Protein. Kirschner and co-workers suggested that immobilization of the chain termini might have been an evolutionary strategy for increasing the stability of proteins, such as those from thermophilic organisms (*37*).

For *Bc*-Csp, we had found that, in fact, two residues near the termini, Arg3 and Leu66, are responsible for its increased equilibrium stability. They contribute additional hydrophobic and electrostatic interactions, and remove an unfavorable Coulombic repulsion between Glu3 and Glu66, which is present in the mesophilic homologue (*24*). The results presented here show that the N-terminal chain region is also of crucial importance for the folding kinetics.

The high Φ_{UN} values obtained for Gln2 and Arg3 from the folding kinetics show that their contributions to stability are largely present already in the transition state. Coulombic interactions play a major role here, because the difference in the refolding rate between *Bc*-Csp and *Bs*-CspB is strongly reduced in the presence of salt. Glu66 shows a low Φ_{UN} value, which indicates that, unlike the N-terminal residues, the C-terminus hardly contributes to the stabilization of the folding transition state.

Φ_{UN} values are composite numbers that report on all interactions of a particular residue in the activated state of folding, or, in our case, on all differences between corresponding residues in the thermophilic and mesophilic variants. Φ_{UN} values of 1 are obtained only when all interactions of a particular residue are as strong as in the native protein, a condition that is rarely met, even when structural probes suggest a nativelike environment for a particular residue (*39*).

Double-mutant cycles (*40*) are used to examine how individual interactions between residues develop during the course of folding. Positions 3, 46, and 66 are close to each other in the native cold shock proteins, and a triple-mutant analysis of the equilibrium stability had shown that Glu residues at positions 3 and 66 or at positions 3 and 46 destabilize the protein electrostatically by 4 kJ/mol each. Glu residues at positions 46 and 66 do not interact (*26*, *32*). The kinetic analysis of the triple-mutant cube confirmed that positions 46 and 66 also do not interact in the transition state. The Coulombic interaction between Glu3 and Glu46 is formed early, and 3 out of 4 kJ/mol of the unfavorable interaction energy is present already in the activated state. On the other hand, the interaction between Glu3 and Glu66 develops late. Here only 1 out of 4 kJ/mol of interaction free energy is present already in the transition state.

The N- and C-terminal regions thus contribute differently to the kinetics of folding. The combination of all kinetic results obtained for position 3 in both *Bs*-CspB and *Bc*-Csp at low and high salt indicates that nearly all interactions of residue 3 are present in the transition state already. The nativelike character of position 3 in the transition state is remarkable, because it is a surface residue and shows discrete disorder in the crystal structure (*25*, *32*).

Position 66 establishes most of its stabilizing hydrophobic interactions only after the transition state. The Leu66Glu mutation destabilizes the native state of *Bc*-Csp by 5.2 kJ/mol in a salt-independent fashion, but the transition state is destabilized by only 1 kJ/mol. Together with the finding that the repulsion between Glu3 and Glu66 develops late in the folding of *Bs*-CspB, this confirms that position 66 is still largely unfolded when the transition states are reached in the folding of both *Bs*-CspB and *Bc*-Csp.

The strong influence of the electrostatic interactions on Csp folding also explains why we previously found similar refolding rates for the wild-type forms of *Bs*-CspB and *Bc*-Csp (*23*). These experiments had to be performed in GdmCl, and this ionic denaturant screened the Coulombic interactions and thus their influence on the refolding kinetics. Only the nonionic interactions persisted, and they are formed predominantly after the transition state in refolding.

Our results for the folding of the cold shock proteins indicate that Coulombic interactions can form early on the folding pathway. These interactions are long-range and should be well-suited for stabilizing partially folded molecules with dynamic structure. They thus might be important as early guides of the folding process.

ACKNOWLEDGMENT

We thank T. Oas, R. Goody, J. Reinstein, and the members of our group for discussions about this work.

REFERENCES

1. Jackson, S. E., and Fersht, A. R. (1991) *Biochemistry 30*, 10428−10435.
2. Viguera, A. R., Martinez, J. C., Filimonov, V. V., Mateo, P. L., and Serrano, L. (1994) *Biochemistry 33*, 2142−2150.
3. Schindler, T., Herrler, M., Marahiel, M. A., and Schmid, F. X. (1995) *Nat. Struct. Biol. 2*, 663−673.
4. Burton, R. E., Huang, G. S., Daugherty, M. A., Fullbright, P. W., and Oas, T. G. (1996) *J. Mol. Biol. 263*, 311−322.
5. Jackson, S. E. (1998) *Folding Des. 3*, R81−R91.
6. Grantcharova, V., Alm, E. J., Baker, D., and Horwich, A. L. (2001) *Curr. Opin. Struct. Biol. 11*, 70−82.
7. Otzen, D. E., Itzhaki, L. S., Elmasry, N. F., Jackson, S. E., and Fersht, A. R. (1994) *Proc. Natl. Acad. Sci. U.S.A. 91*, 10422−10425.
8. Grantcharova, V. P., Riddle, D. S., Santiago, J. V., and Baker, D. (1998) *Nat. Struct. Biol. 5*, 714−720.
9. Martinez, J. C., and Serrano, L. (1999) *Nat. Struct. Biol. 6*, 1010−1016.
10. Baldwin, R. L. (1995) *J. Biomol. NMR 5*, 103−109.
11. Baldwin, R. L., and Rose, G. D. (1999) *Trends Biochem. Sci. 24*, 77−83.
12. Baldwin, R. L., and Rose, G. D. (1999) *Trends Biochem. Sci. 24*, 26−33.
13. Bryngelson, J. D., Onuchic, J. N., Socci, N. D., and Wolynes, P. G. (1995) *Proteins: Struct., Funct., Genet. 21*, 167−195.
14. Dobson, C. M., Sali, A., and Karplus, M. (1998) *Angew. Chem. 37*, 868−893.
15. Dobson, C. M., and Karplus, M. (1999) *Curr. Opin. Struct. Biol. 9*, 92−101.
16. Matthews, C. R. (1987) *Methods Enzymol. 154*, 498−511.
17. Fersht, A. R. (1995) *Curr. Opin. Struct. Biol. 5*, 79−84.
18. Fersht, A. R. (1993) *FEBS Lett. 325*, 5−16.
19. Horovitz, A., and Fersht, A. R. (1992) *J. Mol. Biol. 224*, 733−740.
20. Grantcharova, V. P., Riddle, D. S., and Baker, D. (2000) *Proc. Natl. Acad. Sci. U.S.A. 97*, 7084−7089.
21. Gunasekaran, K., Eyles, S. J., Hagler, A. T., and Gierasch, L. M. (2001) *Curr. Opin. Struct. Biol. 11*, 83−93.
22. Reid, K. L., Rodriguez, H. M., Hillier, B. J., and Gregoret, L. M. (1998) *Protein Sci. 7*, 470−479.
23. Perl, D., Welker, C., Schindler, T., Schröder, K., Marahiel, M. A., Jaenicke, R., and Schmid, F. X. (1998) *Nat. Struct. Biol. 5*, 229−235.
24. Perl, D., Mueller, U., Heinemann, U., and Schmid, F. X. (2000) *Nat. Struct. Biol. 7*, 380−383.
25. Mueller, U., Perl, D., Schmid, F. X., and Heinemann, U. (2000) *J. Mol. Biol. 297*, 975−988.
26. Perl, D., and Schmid, F. X. (2001) *J. Mol. Biol. 313*, 343−357.
27. Schindelin, H., Herrler, M., Willimsky, G., Marahiel, M. A., and Heinemann, U. (1992) *Proteins: Struct., Funct., Genet. 14*, 120−124.

28. Mayr, L. M., Landt, O., Hahn, U., and Schmid, F. X. (1993) *J. Mol. Biol. 231*, 897−912.
29. Jacob, M., Holtermann, G., Perl, D., Reinstein, J., Schindler, T., Geeves, M. A., and Schmid, F. X. (1999) *Biochemistry 38*, 2882−2891.
30. Clegg, R. M., and Maxfield, B. W. (1976) *Rev. Sci. Instrum. 47*, 1383−1392.
31. Schindler, T., and Schmid, F. X. (1996) *Biochemistry 35*, 16833−16842.
32. Delbrück, H., Mueller, U., Perl, D., Schmid, F. X., and Heinemann, U. (2001) *J. Mol. Biol. 313*, 359−369.
33. Jacob, M., Schindler, T., Balbach, J., and Schmid, F. X. (1997) *Proc. Natl. Acad. Sci. U.S.A. 94*, 5622−5627.
34. Jacob, M., Geeves, M., Holtermann, G., and Schmid, F. X. (1999) *Nat. Struct. Biol. 6*, 923−926.
35. Jacob, M., and Schmid, F. X. (1999) *Biochemistry 38*, 13773−13779.
36. Perl, D., Jacob, M., Bánó, M., Stupák, M., Antalík, M., and Schmid, F. X. (2001) *Biophys. Chem.* (in press).
37. Makhatadze, G. I., and Privalov, P. L. (1992) *J. Mol. Biol. 226*, 491−505.
38. Hennig, M., Darimont, B., Sterner, R., Kirschner, K., and Jansonius, J. N. (1995) *Structure 3*, 1295−1306.
39. Bulaj, G., and Goldenberg, D. P. (2001) *Nat. Struct. Biol. 8*, 326−330.
40. Horovitz, A. (1996) *Folding Des. 1*, R121−R126.
41. Kraulis, P. J. (1991) *J. Appl. Crystallogr. 24*, 946−950.

BI011378S